Palaeogeography, Palaeoclimatology, Palaeoecology 565 (2021) 110191

Contents lists available at ScienceDirect

Palaeogeography, Palaeoclimatology, Palaeoecology

journal homepage: www.elsevier.com/locate/palaeo

Biogeochemical evolution and organic carbon deposition on the Northwestern European Shelf during the Toarcian Ocean Anoxic Event

Alexander J.P. Houben [a], Tatiana Goldberg [a,b,*], Caroline P. Slomp [c]

[a] TNO Geological Survey of the Netherlands, Utrecht, the Netherlands
[b] GFZ - German Research Centre for Geosciences, Telegrafenberg, 14473 Potsdam, Germany
[c] Department of Earth Sciences, Utrecht University, Utrecht, the Netherlands

ARTICLE INFO

Keywords:
T-OAE
Primary productivity
Organic matter
Redox
Palynofacies
Fe-speciation

ABSTRACT

The Toarcian Oceanic Anoxic Event (T-OAE, ~183 Ma) represents a well-known episode of organic-rich deposition, which is accompanied by a substantial negative carbon-isotope excursion (CIE). Underpinning the relationships between the carbon-cycle perturbation, ocean anoxia, primary productivity feedbacks and the enrichment of sedimentary organic carbon remains a major challenge. Here, we present high-resolution geochemical, palynological and organofacies data from three lower Toarcian successions from the NW European shelf, spanning the T-OAE. Chronostratigraphic calibration of the successions is achieved through organic carbon isotope ($\delta^{13}C$) records. Iron-speciation and major and trace-element data indicate that bottom-waters were euxinic and intermittently anoxic-ferruginous prior to, throughout and beyond the CIE. In terms of organofacies and palynological composition, the CIE-interval is dominated by dense clusters of amorphous organic matter containing abundant small spherical prasinophyte cysts (*Halosphaeropsis liassica)*. The peak CIE is bracketed by a major increase in abundance of prasinophycean vegetative cysts (*Tasmanites* and *Pleurozonaria* spp.). On the basis of their modern physiology, this suggests shoaling of the chemocline into the photic zone. The combined proxy data suggest a scenario in which anoxygenic photosynthetic productivity proliferated in nutrient-rich, anoxic to seasonally euxinic surface-waters of the stratified NW-European shelf during the CIE. A return to oxic-marine conditions is recorded by the recurrence of organic-walled dinoflagellate cysts in accordance with enhanced water column mixing post CIE. This is concurrent with a gradual termination of strongly stratified conditions across the NW-European shelf.

1. Introduction

Organic matter burial into black shale deposits has major implications for carbon sequestration (Barclay et al., 2010; Xu et al., 2017) for understanding the development of anthropogenically induced anoxia (Stramma et al., 2008; Keeling et al., 2010) and for economic exploitation (Demaison and Moore, 1980; Wignall, 1994). Hence, there is a need to understand the environmental factors contributing to the formation of organic-rich black shales in the past. Although primary productivity by marine organisms is central to organic matter enrichment (Pedersen and Calvert, 1990; Kuypers et al., 2002), the interplay between primary productivity and water column redox conditions is key to understanding organic matter deposition and preservation (e.g., Jenkyns, 2010).

A distinct phase of black shale deposition occurred in the marginal seas of northwestern Europe during the Toarcian Anoxic Event (T-OAE), near the boundary between the *tenuicostatum* and *falciferum* Ammonite zones (Jenkyns, 1988; Hesselbo et al., 2000). The T-OAE is marked by a worldwide coeval negative carbon isotope excursion (CIE) recorded in carbonate, bulk organic carbon and fossil wood (Jenkyns, 1988; Hesselbo et al., 2000; Röhl et al., 2001; Suan et al., 2011; Them et al., 2017a; Xu et al., 2017; Fantasia et al., 2018; Izumi et al., 2018). The negative CIE was proposed to have been driven by the addition of a ^{12}C-enriched carbon source to the ocean-atmosphere reservoir. Several mechanisms have been suggested ranging from magmatic intrusions and metamorphic alteration of organic deposits (McElwain et al., 2005), and/or methane input through hydrate dissolution (Hesselbo et al., 2000), wetland instability (Them et al., 2017b) and permafrost areas (Ruebsam et al., 2019).

Strong increases in atmospheric greenhouse gasses and global

* Corresponding author at: GFZ - German Research Centre for Geosciences, Potsdam, Germany
E-mail addresses: alexander.houben@tno.nl (A.J.P. Houben), goldberg@gfz-potsdam.de (T. Goldberg), C.P.Slomp@uu.nl (C.P. Slomp).

https://doi.org/10.1016/j.palaeo.2020.110191
Received 23 July 2020; Received in revised form 18 December 2020; Accepted 19 December 2020
Available online 25 December 2020

climate warming were recorded in the latest Pleinsbachian and Early Toarcian (McElwain et al., 2005; Suan et al., 2008; Gómez and Goy, 2011; Korte et al., 2015). The warming resulted in high precipitation rates, increased weathering and terrestrial run-off (Cohen et al., 2004; Montero-Serrano et al., 2015; Percival et al., 2016; Them et al., 2017b). This was proposed to have led to high nutrient supply to the marginal seas triggering a rise in primary productivity (Jenkyns et al., 2001; Slater et al., 2019).

Enhanced primary productivity leads to oxygen consumption upon organism decay and was proposed as the mechanism of deoxygenation of the marginal Early Toarcian seas (Jenkyns et al., 2001; Ruebsam et al., 2018; Slater et al., 2019). However, a number of other factors are considered as initiators of marine deoxygenation during T-OAE, such as sluggish ocean circulation and decreasing water column mixing in a warming climate and salinity stratification resulting from increased fresh-water run-off (Röhl et al., 2001; Cohen et al., 2007; Danise et al., 2013; McArthur et al., 2008; Dera and Donnadieu, 2012; Remírez and Algeo, 2020a).

Organic matter deposition and oxygen depletion are predominantly expressed in the semi-restricted European epicontinental seas which comprise the Laurasian Seaway (e.g., Bjerrum et al., 2001; Ruebsam et al., 2018). Various studies point to spatial differences in water column redox conditions on the northwestern European shelf, with the more restricted shelf in the north being characterized by anoxic bottom waters and the southern shelf remaining mostly oxygenated (e.g., Ruvalcaba Baroni et al., 2018). Contrarily, in some northwestern European sections, sedimentological evidence suggested that oxic conditions prevailed and were only sporadically interrupted by bottom water anoxia (Ghadeer and Macquaker, 2011; Trabucho-Alexandre et al., 2012). The degree and distribution of the marine deoxygenation during the CIE, as well as its cause remain a matter of debate.

Geochemical evidence of bottom-water anoxia on the European shelf associated with the T-OAE is provided by sediment enrichments in redox sensitive elements, such as Fe, Mo, U, V and Cr (e.g., Pearce et al., 2008; Jenkyns, 2010; Hermoso et al., 2013), elevated ratios of organic carbon to phosphorus (C_{org}/P; Montero-Serrano et al., 2015, Ruvalcaba Baroni et al., 2018), a high degree of pyritisation (McArthur et al., 2008) and on the basis of stable metal isotopes (Pearce et al., 2008; Dickson et al., 2017; Them et al., 2018). Photic zone euxinia (i.e., waters in the photic zone containing H_2S) has mainly been deduced from organic molecular biomarkers such as isorenieratane and chlorobactane (Summons and Powell, 1987; Schouten et al., 2000; Bowden et al., 2006; van Breugel et al., 2006; French et al., 2014; Ruebsam et al., 2018). Palynomorph assemblages, particularly the abundance of prasinophyte cysts, may indicate changes in redox conditions of the upper water column (Prauss and Riegel, 1989; van de Schootbrugge et al., 2013). Based on the presence of the palynomorph *Halosphaeropsis liassica,*Bucefalo Palliani et al. (2002) suggested that shoaling of the oxygen minimum zone controlled the surface-water paleoecology and thereby contributed to the development of the organic-rich deposits during the T-OAE. Quantitative palynological analyses provide a way to assess the direct provenance of sediment organic matter (e.g., marine vs. terrestrial). In addition, the composition of marine palynological associations may provide clues for ecological turnover in the photosynthetic community in surface waters.

In this study, we investigate the feedbacks between bottom water redox conditions, organofacies and palynological assemblage variations that contributed to organic carbon burial during T-OAE. We present high-resolution palynological and geochemical data from the West Netherlands Basin (NL), Dutch Central Graben (NL) and Cleveland Basin (UK, see Fig. 1). Chronostratigraphic calibration of the successions is achieved through generation and compilation of organic $\delta^{13}C$-records. Combined, this allows a reconstruction of temporal and shelf-wide variations in redox conditions and their relationship with organic provenance, as well as changes in the photosynthetic ecosystem in waters overlying the northwestern European epicontinental shelf.

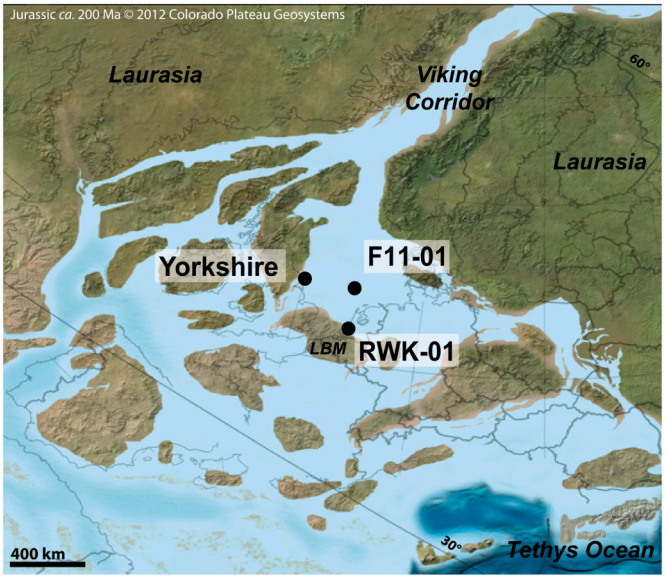

Fig. 1. Paleogeographic reconstruction of the NW-European Shelf during the Jurassic. The locations of the three study sites are depicted by black dots. Note that the London Brabant Massif (LBM), in the vicinity of RWK-01 was likely largely submerged during Toarcian times. This figure was modified from Ruvalcaba Baroni et al. (2018) and uses the paleogeographic map of Ron Blakey, Deep Time MapsTM, https://deeptimemaps.com/gmedia-album/.

2. Geological setting

Coupled with local tectonic subsidence and rising sea levels, a shallow epicontinental sea was established between Laurentia and Eurasian landmasses by Early Jurassic times (e.g., Wignall and Hallam, 1991). This sea extended from the present-day UK into the Netherlands, Germany and into central Poland (Fig. 1). Towards the southwest, the European Epicontinental Sea (EES) was open towards the Tethyan Ocean, whereas the northwestern part of the EES was marginally connected via the Viking Corridor to the Arctic Sea (van de Schootbrugge et al., 2019) and possibly via the Hispanic Corridor to the Panthalassic Ocean (Correia et al., 2017).

In the UK sector of the Southern North Sea Basin, the Lower Jurassic Lias Group is about 400 m thick and part of the fault-bounded Cleveland and Sole Pit basins (Powell, 2010). It is predominantly composed of a rather monotonous sequence of grey calcareous mudstones and argillaceous micritic limestones, with thin beds of ooidal, chamositic and sideritic ironstone deposited during Sinemurian and Pliensbachian times (Hesselbo and Jenkyns, 1995). Lower Toarcian bituminous shales (Jet Rock unit of the Mulgrave Shale Member of the Whitby Mudstone Formation) are locally developed in the Cleveland Basin. Upper Toarcian sediments are absent over much of eastern England due to a pre-Aalenian erosional phase (Wignall and Hallam, 1991). Further to the west in the Netherlands, Lower Jurassic rocks belong to the Aalburg (Hettangian-Pliensbachian), Posidonia Shale (Lower Toarcian) and the Upper Toarcian to Bajocian Werkendam Formations (TNO-GDN, 2020). Their distribution is restricted to Mesozoic graben structures, including the offshore parts of the Dutch Central Graben and the onshore West Netherlands Basin. The Hettangian to Toarcian successions comprise mainly dark grey to black, variably calcareous, marine mudstones and claystones. The upper part of the Lower Jurassic succession in the Netherlands is variably truncated due to uplift and erosion during mid-Jurassic times (Doornenbal and Stevenson, 2010).

3. Materials and methodology

3.1. Materials

3.1.1. Cleveland Basin (Yorkshire Coast)

The Lower Toarcian succession was sampled at an exposure near the town of Runswick Bay (54° 31′ 4″ N, 0° 44′ 5″ W; WGS84). A total of 65 samples were collected across 11.5 m, with a resolution of ~6 samples per meter, from the upper Grey Shale Member (corresponding to the *tenuicostatum* ammonite Zone), the (informal) Jetrock and the Bituminous Shales units belonging to the Mulgrave Shale Member (corresponding to the *falciferum*Zone). The Grey Shale Member consists of grey siltstones to silty claystones showing a generally scarce development of stratification and lamination at outcrop scale, with intercalated levels of diagenetic nodular carbonates (siderite and dolomite). The organic-rich Mulgrave Shale Member can be distinguished from the Grey Shale Member by its finer clayey texture and finely laminated appearance at outcrop scale. The Jet Rock, is particularly enriched in organic matter, reaching up to 18% TOC from an average of ~6% (Jenkyns, 1988) and contains distinct horizons of abundant large calcareous concretions (Hallam, 1962; Coleman and Raiswell, 1981). The Bituminous Shales unit represents a gradual return to slightly coarser sediments.

The above-mentioned stratigraphy is clearly manifested by distinct marker beds in the field. These marker beds were used for correlation of the samples taken for this study to the published carbon isotope reference curves of Cohen et al. (2004) and Kemp et al. (2005). These marker beds are the "Cannonball Doggers" approximating the base of the Mulgrave Shale Mb. (and the Jet Rock), the "Whalestones" level in the middle of the Jet Rock, the "Curling Stones" level within the Jet Rock and the "Top Jet Dogger" and "Millstones" approximating the top of the Jet Rock (Fig. 2). A more detailed description of these marker beds is provided by and Hesselbo and Jenkyns (1995) and references therein.

3.1.2. Dutch Central Graben (Well F11-01)

Well F11-01 is located at 54° 22' 1.4″ N, 4° 35' 34″ E (WGS84), near the southern margin of the Dutch Central Graben. During the Early Jurassic, the well location was in a relatively distal setting in a subsiding graben system. The well was drilled in 1970 and retrieved a cored section from the Posidonia Shale Formation between 2657 and 2672 m along-hole depth. Only the lower part of the Posidonia Shale Formation was recovered, which is considered to be equivalent to the *tenuicostatum* and *falciferum* ammonite Zones (Trabucho-Alexandre et al., 2012). The overall lithology consists of very dark grey to black mudstones. Horizontally continuous fibrous calcite and cone-in-cone structures are recorded in the upper part of this core (above 2662.6 m depth, Trabucho-Alexandre et al., 2012). A total of 31 samples was collected from a 15 m interval, yielding a sample resolution of 2 samples per meter/50 cm.

3.1.3. West Netherlands Basin (Well Rijswijk-1)

Well Rijswijk-1 was drilled in 1952 in the town of Rijswijk, the Netherlands (52° 1' 30.6″ N, 4° 18' 35.7″ E; WGS84). In this well, three cored sections were recovered across the Pliensbachian Aalburg and Toarcian Posidonia Shale Formations. An upper section was recovered between 2075 and 2081 m along-hole depth where a total of 10 samples was collected (resolution of ~1 sample per 60 cm). The middle-cored

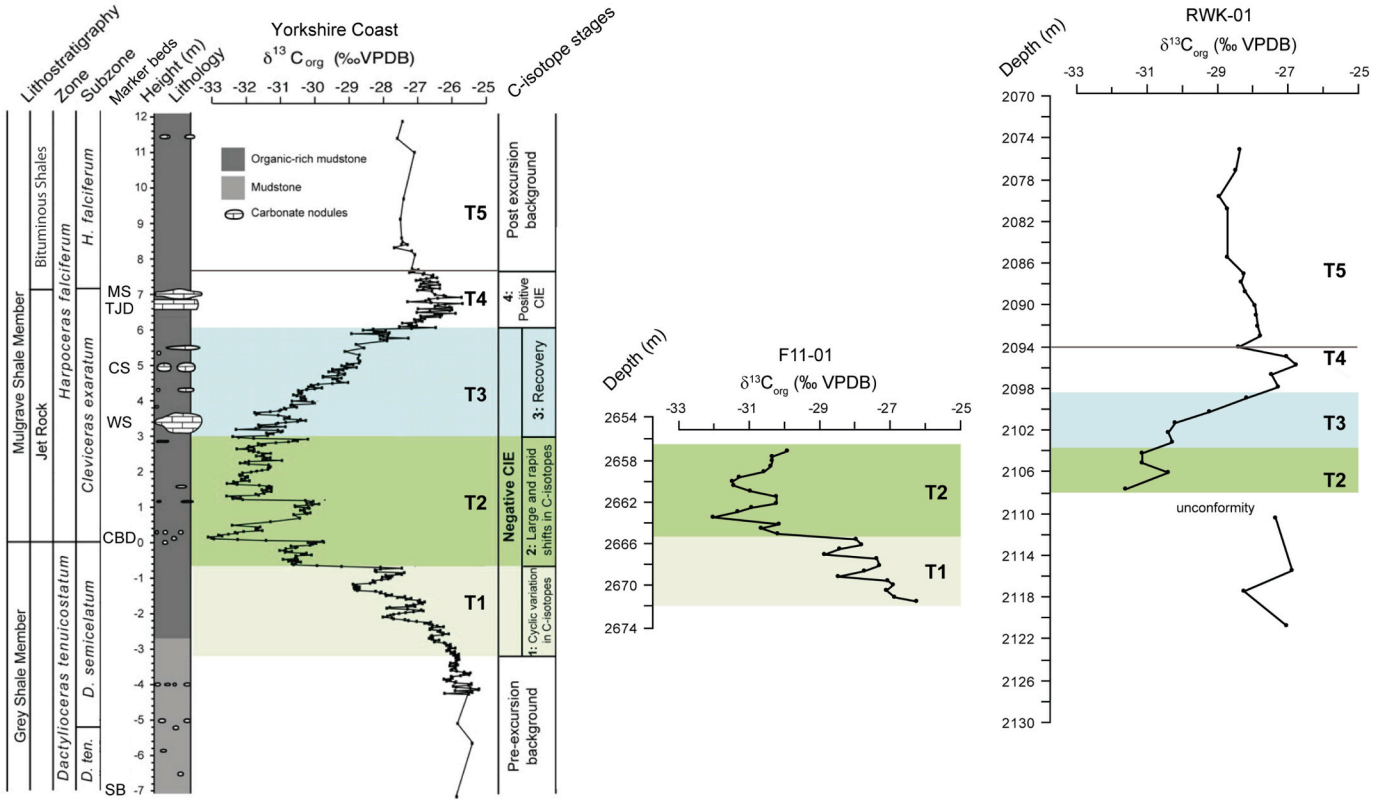

Fig. 2. Bulk organic carbon isotope records for the Yorkshire succession (after Kemp et al., 2011) and the two wells from the Netherlands. The samples for the Yorkshire succession were linked to the carbon isotope dataset by identifying the following marker beds: "Cannon Ball Doggers" (CBD), the "Whalestones" (WS), the "Curling Stones" (CS), the "Top Jet Dogger" (TJD) and the "Millstones" (MS). The shaded intervals and grey lines indicate the isotope stages that illustrate the carbon isotope excursion: light green indicates the initial excursion, darker green the maximum excursion, blue the recovery and the white delineated by the grey line the positive shift following the excursion (see also Kemp et al., 2011). The isotope stages are numbered T1 to T5 and described further in the text. The cored section in well F11-01 corresponds to the initial excursion and the maximum excursion values whereas well RWK-01 captures the recovery, positive excursion and the interval overlying the CIE. (For interpretation of the references to colour in this figure legend, the reader is referred to the web version of this article.)

segment (2085–2110 m depth) is the most expanded and continuous. From the middle interval 46 samples were collected, at a resolution of ~2 samples per meter. At 2108 m a fault runs through the core implying that downhole the transition to the Aalburg Formation is not complete. A lower segment (below the fault) was recovered between 2110 and 2121 m depth, form which 6 more samples were collected. The sediments consist mainly of black to grey, finely laminated to bedded, fine-grained siliciclastics with some intercalated marls.

3.2. Stable isotope and inorganic geochemical analyses

Carbon isotopes were determined on a continuous flow isotope ratio mass spectrometer (Europa Scientific 20–20 IRMS) with dual inlet, connected to an elemental analyser (EA-IRMS) at IsoAnalytical Ltd. Sample powders were pre-treated with 4 M HCl to remove the carbonate phases. Reproducibility, as determined via replicate measurements of 20% of the samples, was ±0.1‰ (1sd). The carbon isotope values are referenced against the Vienna Pee Dee Belemnite international reference material. Internal reference materials IA-R001 (wheat flour, $\delta^{13}C = -26.43‰$), IA-R005 (beet sugar, $\delta^{13}C = -26.03‰$) and IA-R006 (cane sugar $\delta^{13}C = -11.64‰$) were used for quality control. TOC was analysed both with EA-IRMS and with a LECO-CS230 analyser after removal of carbonate with 4 M HCl. Both methods provided comparable results (Table S1). Analytical error on TOC was ≤5% (relative standard deviation). Major elements were measured via XRF on fused-beads (Li-metaborate) for F11-1 and RWK-01 and via ICP-OES on fused-bead leachates for Yorkshire coast sediments (at Chemostrat Ltd.). Mo and U were measured with an ICP-MS on fused-bead leachates. Uncertainly based on replicate reference materials was better than 7% (relative standard deviation) for elements measured via ICP-OES, less than 12% for ICP-MS and less than 10% for XRF. The Fe-speciation analyses were performed at Utrecht University. The contents of Fe-carbonate, Fe-oxides and -hydroxides and Fe-magnetite were determined using a sequential extraction scheme (Poulton and Canfield, 2005). For the final extraction step Fe-pyrite was dissolved with concentrated nitric acid in a 2-h extraction at room temperature. Fe concentrations were measured photometrically. Pyrite extraction was also determined on 4 samples via the hot chromium chloride extraction technique from Canfield et al. (1986). Both methods resulted in comparable concentrations of pyrite Fe (Table S1).

3.3. Palynology and organofacies analyses

For palynological and organofacies analyses, rock samples were treated with a 30% HCl solution and a 35% HF solution. The remains were sieved with a 250 μm and subsequently a 10 μm mesh sieve. The organic residues of the 10 μm fraction were mounted on glass slides in glycerine jelly. No oxidation steps were applied to preserve the original state of the organic matter. Two suites of analyses were performed, one aimed at identifying the visual organic matter assemblages (here further referred to as organofacies analyses), thereby focussing on palynoclast groups and the next analytical suite focussed on the palynomorph assemblage composition. For both analytical suites, at least 200 specimens were identified using the 40× and 63× objectives.

For the organofacies analyses we differentiated three groups; AOM Type-1, AOM Type-2 and wood. Type 1 is almost translucent under transmissive light and is, in general, less massive than Type 2. Type 2 is not translucent, darker and more massive than Type 1. The last group of palynoclasts consists of organic matter particles that can be attributed to wood remains. Three types are distinguished, based on their coloration, opacity and the appearance of vascular structures.

Palynomorphs were grouped into several classes; pollen and spores (sporomorphs), organic-walled dinoflagellate cysts and prasinophyte algae. To be able to quantify palynomorphs encased in AOM-clusters, reflective ultra-violet light microscopy was performed. Because the encountered AOM is very weakly UV-fluorescent compared to the palynomorphs, the latter become clearly visible. Notably, acritarchs and remains of prasinophyte algae are strongly fluorescent but also sporomorphs have a characteristic UV-reflectance frequency which allows them to be quantified in the AOM-clusters.

4. Results and interpretation

4.1. Carbon isotope stratigraphy

The high-resolution organic bulk-carbon isotope record from the exposures in the Cleveland Basin (Cohen et al., 2004, 2007; Kemp et al., 2005, 2011) delineates an evident series of shifts across the Grey Shale Member and Mulgrave Shale Member. These form the framework for stratigraphic correlation of wells F11-01 and RWK-01 in the Netherlands (Fig. 2). We distinguish five isotope stages, here referred to as T1 to T5. These stages correspond to the initial negative carbon isotope excursion of the *semicelatum* Subzone of *tenuicostatum* Zone (T1), maximum negative $\delta^{13}C$ values of the *exaratum* Subzone of the *falciferum* Zone (T2), recovery towards higher $\delta^{13}C$ values (T3), small positive excursion (T4) and stable $\delta^{13}C$ throughout the remainder of the *falciferum* Subzone (T5). The isotope stages T1 to T3 span the negative Toarcian CIE. There is no precise stratigraphic definition for the T-OAE. In the Yorkshire Coast section, the T-OAE is considered to correspond to the interval covered by our stages T1 to T4 (see Remírez and Algeo, 2020b for an overview).

The isotope stages are used to chronostratigraphically compare the three studied sites. The two cores from the Netherlands do not completely capture the CIE. In Well F11-01, an evident negative shift (of 4 to 5‰) is recorded (Fig. 2). Arguably, a few smaller scale cyclical shifts are also observed. The interval consequently corresponds to isotope stages T1 and T2. The top of core F11-01 ends in the middle of the *exaratum* Subzone (Fig. 2). In Well RWK-01, the base of the core is compromised by faulting. Indeed, the lowermost samples are characterized by relatively heavy and stable values, supporting assignment to the Pliensbachian Aalburg Formation. The overlying interval above 2108 m depth clearly reflects a 4 to 5‰ positive carbon isotope shift, followed by a 0.5‰ positive shift at 2095 m depth, akin to the positive shift associated with the *exaratum* - *falciferum* Subzone boundary in the Cleveland Basin (T4).

4.2. Bottom-water redox indicators

The use of sediment Fe-speciation as a local palaeoredox indicator is based on the presence or absence of enrichments in (bio)geochemically available Fe minerals (Raiswell and Canfield, 1998; Poulton and Raiswell, 2002; Poulton and Canfield, 2011). Highly reactive iron (Fe_{HR}) comprises ferric oxides, iron carbonates, magnetite and pyrite. A highly reactive iron to total ratio (Fe_{HR}/Fe_T) of below 0.38 indicates an oxygen containing water column above the sediment, whereas values above this threshold provide strong evidence for anoxic depositional conditions. The extent of pyritisation of the highly reactive Fe pool (Fe_P/Fe_{HR}) indicates whether the bottom water was anoxic and ferruginous (Fe-rich) or euxinic, provided that the Fe_{HR}/Fe_T is above 0.38. Fe_P/Fe_{HR} values below 0.7 reflect ferruginous water column conditions. The threshold between anoxic-ferruginous and euxinic bottom water conditions is less well defined and is set between 0.7 and 0.8 (Anderson and Raiswell, 2004; März et al., 2008; Poulton and Canfield, 2011). When Fe_P/Fe_{HR} indicates sulfidic conditions but Fe_{HR}/Fe_T is below 0.38 (sign of oxic to dysoxic bottom water) H_2S production is thought to occur close to but below the sediment/water interface. The use of these proxies needs to be assessed carefully. In carbonate rich strata the incorporation of Fe^{2+} into diagenetic carbonate may lead to an overestimation of anoxia when Fe-speciation is applied to sediments with low Fe_T contents, i.e., <0.5% (Clarkson et al., 2014). This feature is often accompanied by high organic S contents, commonly termed 'excess S' (Tessin et al., 2016).

Redox sensitive trace elements change their charge and/or

speciation with varying redox conditions thus decreasing their solubility from oxic to anoxic/sulphidic conditions (Brumsack and Gieskes, 1983; Algeo, 2004; Tribovillard et al., 2006). While U experiences a valence change with the transition to anoxic conditions, Mo undergoes a species as well as oxidation state change with reducing conditions and is particularly sensitive to the H_2S concentration (Anderson et al., 1989; Zheng et al., 2000; Helz et al., 2004). The molar ratios of organic carbon over phosphorus have also been proposed as a local bottom water redox indicator (e.g., Algeo and Ignall, 2007). In oxic seawater organic matter is preferentially oxidised, whereas P is preferentially retained via precipitation as fluorapatite or fixation to Fe-(oxyhydr)oxides and the increased ability of bacteria to store P in well-oxygenated environments (Ingall et al., 1993). In contrast, in anoxic conditions organic carbon is retained while P is recycled, causing C_{org}/P ratios to increase with oxygen depletion (Mort et al., 2008; Tsandev and Slomp, 2009; Kraal et al., 2010). This proxy should be treated with caution, as the carbon/phosphorus ratio is also influenced by the type of organic matter, detrital P input, preservation of biogenic Ca-P and burial diagenesis (Algeo and Ignall, 2007; Kraal et al., 2010).

4.2.1. *Cleveland Basin - Yorkshire Coast*

Throughout the analysed Yorkshire Coast section, Fe-speciation points to persistent anoxic bottom water conditions, with $Fe_{HR}/Fe_T > 0.38$ (Fig. 3). However, short-lived oxic intervals on a seasonal or annual scale cannot be resolved with the current sampling resolution. Fe_P/Fe_{HR} is mostly at the threshold to euxinic conditions (0.7 to 0.8), indicating that hydrogen sulphide was present in bottom waters, albeit not permanently. Incorporation of Fe^{2+} into diagenetic carbonate does not affect the redox proxy because total Fe is well above 0.5 wt%, even in the carbonate rich strata.

C_{org}/P increases significantly from the Grey Shales Member towards the Jet Rock unit (isotope stages T1 to T2) and decreases again towards the Bituminous Shales unit in isotope stages T3 to T5 (Fig. 3). Overall, C_{org}/P in this section points to anoxic conditions, except for in the Bituminous Shale unit (isotope stage T5), where C_{org}/P falls partially below 50. To account for the influence of differential sedimentation and authigenesis, U and Mo were normalised to Al (see also Algeo and Liu, 2020). For most of the succession Mo/Al and U/Al ratios are low and close to those of Post Archean Average Shale (PAAS, Taylor and McLennan, 1985). There is a general co-variation of Mo and U with TOC exemplifying their preferential fixation to organic matter (e.g., Chappaz et al., 2014). U/Al and Mo/Al values increase in isotope stage T3, mimicking the TOC behavior in the section (Fig. 3). Redox sensitive trace elements (mainly Mo and U) correlate with high TOC concentrations. When normalised to TOC, the redox sensitive element enrichments during the T-OAE point to their affinity to organic matter (Chappaz et al., 2014) rather than to a variation in the redox conditions. Towards the top of the section (mid isotope stage T4 to T5) Mo deviates from this trend towards higher Mo/Al and Mo/TOC ratios, whereas U/Al remains low.

Based on the Fe-speciation and C_{org}/P, intermittently euxinic conditions dominated the Yorkshire Coast bottom water. Mo, on the other hand, is relatively low during the CIE and only shows significant enrichment in isotope stage T5. This can be generally attributed to the fact that in a restricted basin with widespread euxinic bottom water, Mo is readily lost to the sediment and is not fully replenished due to insufficient water exchange (e.g., Algeo and Lyons, 2006; McArthur et al., 2008; Goldberg et al., 2016; Remírez and Algeo, 2020a). Based on low Mo/TOC ratios, Mo deficiency has been previously inferred for the Cleveland Basin during T-OAE (McArthur et al., 2008; Ruvalcaba Baroni et al., 2018; Dickson et al., 2017; Remírez and Algeo, 2020a; Remírez and Algeo, 2020b). We conclude that Mo/Al variation is not fully diagnostic for the intensity of the local redox conditions.

4.2.2. *West Netherlands Basin Well RWK-01*

Fe-speciation, C_{org}/P and high redox-sensitive trace elements in the Upper Pliensbachian Aalburg Formation (2110–2122 m) point to dysoxic to anoxic bottom-water conditions (Fig. 4). During deposition of the

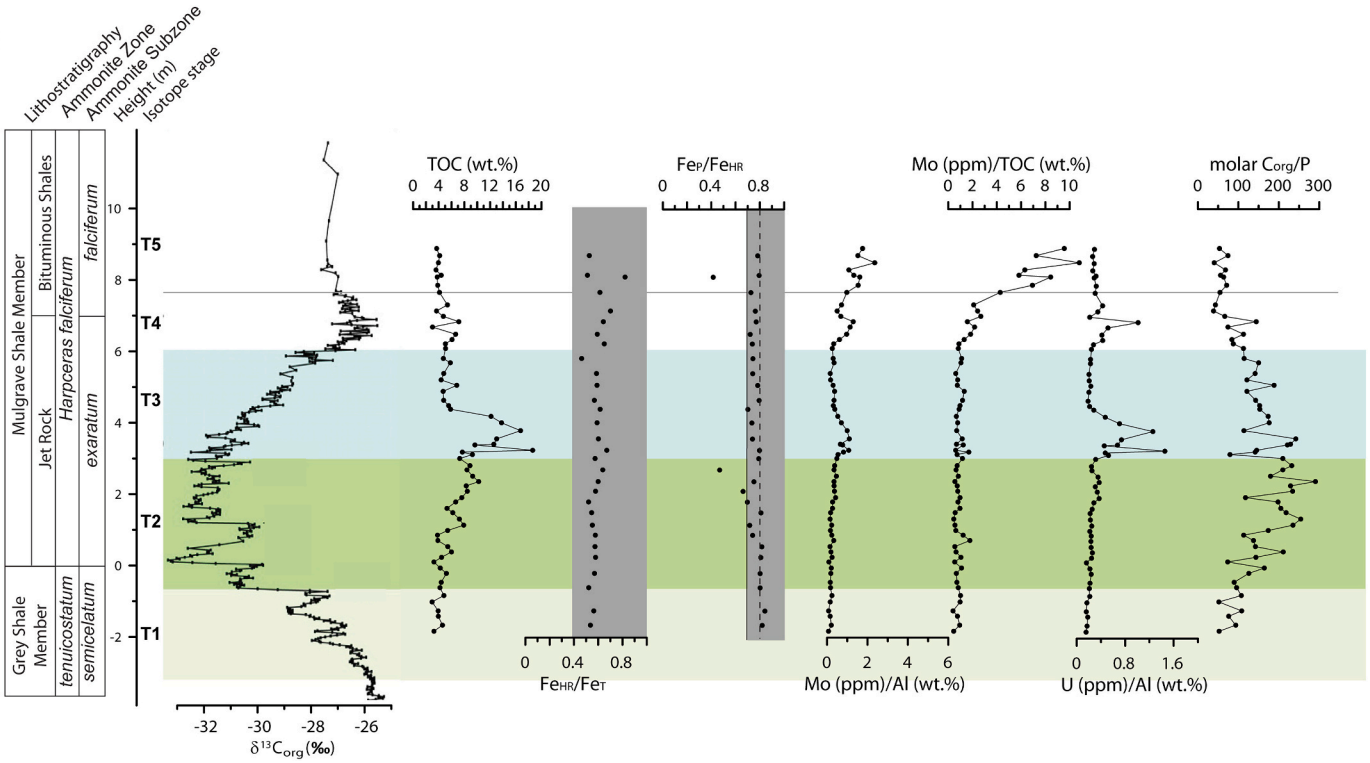

Fig. 3. Fe-speciation and redox-sensitive element ratios plotted along with TOC and the carbon isotope curve (from Kemp et al., 2011) from the Yorkshire Coast, Cleveland Basin, succession. The isotope stages (T1–T5) provide stratigraphic context for comparison to the other records.

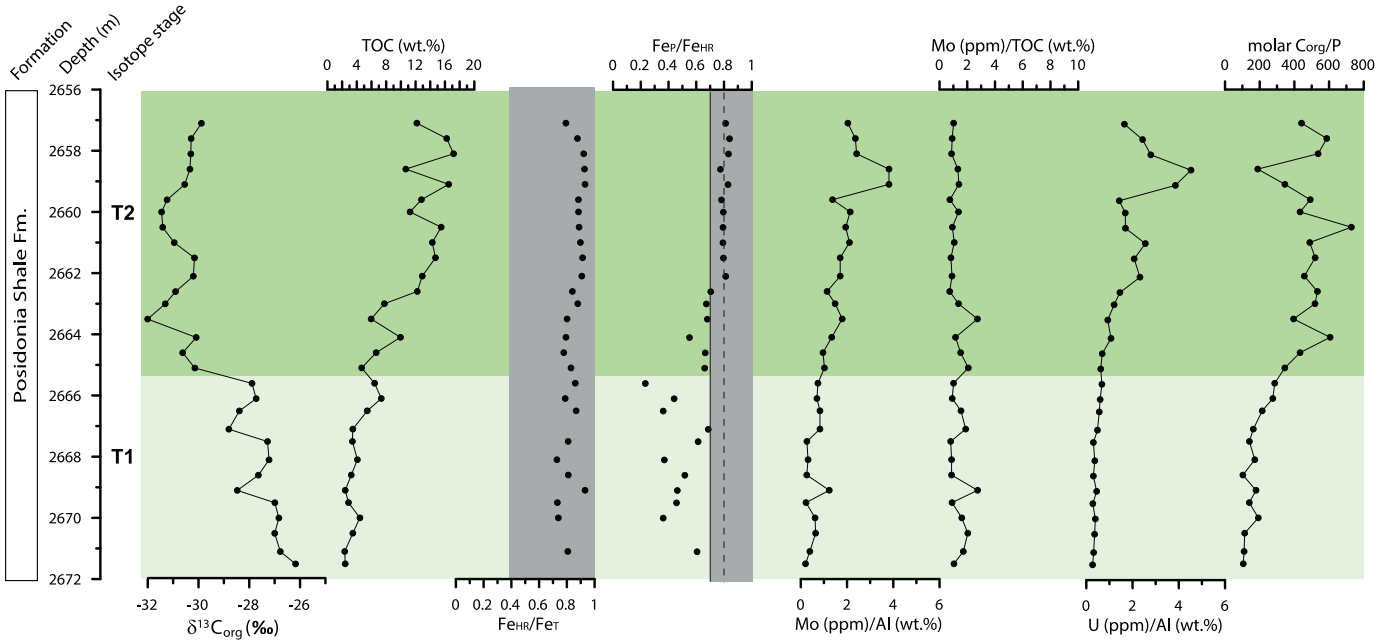

Fig. 4. Fe-speciation and redox-sensitive element ratios displayed along with TOC and the carbon isotopes from Well F11-01. The isotope stages (T1–T2) provide stratigraphic context.

Posidonia Shale Formation (isotope stages T2 to T5), Fe_{HR}/Fe_T indicate initially anoxic-ferruginous ferruginous bottom water conditions that change to sulfidic. Total Fe content is well above 0.5 wt% throughout the entire section. The top part of the Posidonia Shale Formation (stages T3 to T5) is marked by mostly sulfidic bottom water that may have been intermittently anoxic-ferruginous.

Similar to the Yorkshire coast section, U/Al and Mo/Al covary with TOC during isotope stages T2 toT4, exemplifying the preferential fixation of these redox sensitive elements to organic matter (Chappaz et al., 2014). Both Mo/Al and Mo/TOC also increase strongly from isotope stage T4 to T5 (Fig. 4), which indicates that a Mo deficiency during the CIE with a Mo replenishment post T-OAE also occurred in the West Netherlands Basin. C_{org}/P increases from T2 and remains well above the anoxic threshold up until top isotope stage T5. The decline in C_{org}/P at the top of the succession may be influenced by the type of organic matter present or by a decline in the intensity of anoxia.

4.2.3. *Dutch Central Graben Well F11-01*

Similar to the Yorkshire Coast and RWK-01 successions, the Fe-speciation data from Well F11-01 indicate anoxic bottom water conditions throughout isotope stages T1 to T2 (Fig. 5). Fe_T is consistently above 0.5 wt%, thus Fe availability did not affect the validity of the

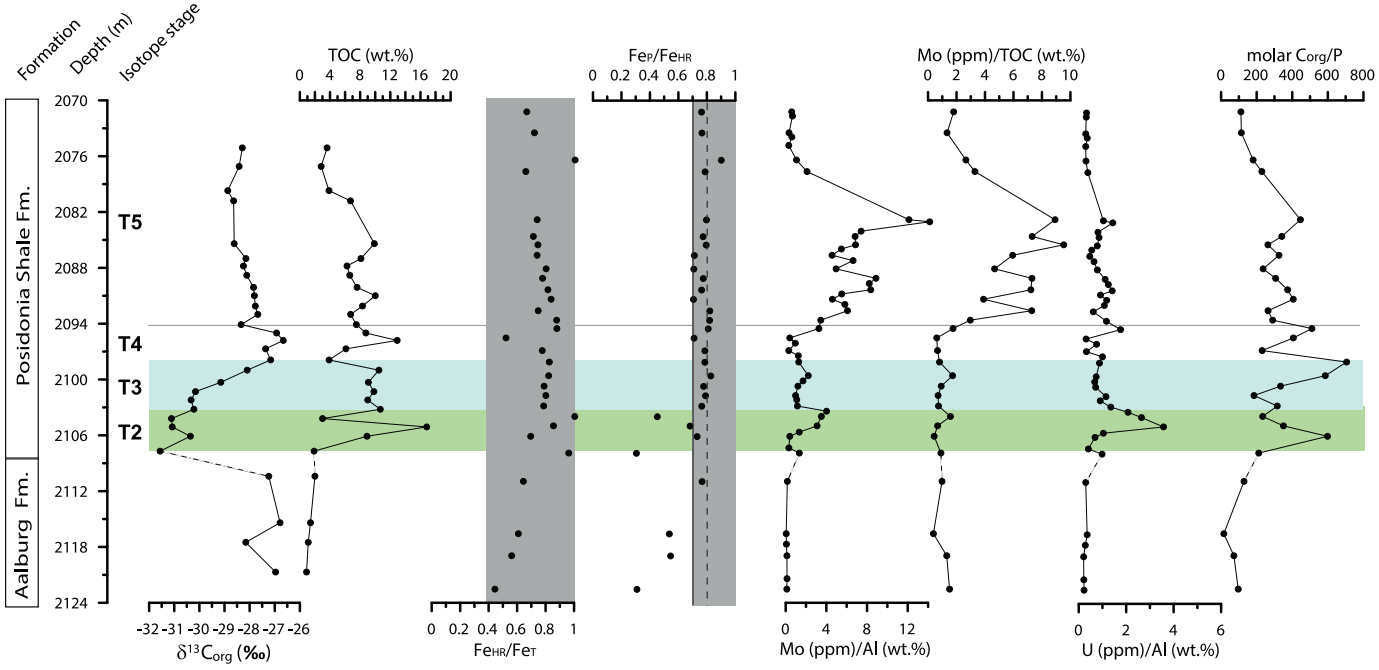

Fig. 5. Fe-speciation and redox-sensitive element ratios displayed along with TOC and the carbon isotopes from well RWK-01. The isotope stages (T2–T5) provide stratigraphic context. Note that the interval corresponding to isotope stage T1 is not present at this location.

Fe_{HR}/Fe_T proxy. Below ~2664 m (isotope stage T1) Fe_P/Fe_{HR} is below 0.7, indicating non-sulfidic conditions. With some fluctuation, Fe_P/Fe_{HR} increases and indicates sulfidic bottom water conditions at the top of the section (isotope stage T2). C_{org}/P increases from ~100 to ~600 during T1 and remains high during T2 (Fig. 5). The trend towards increasing Mo/Al and U/Al ratios can also be seen from T1 to T2. This corresponds with a contemporaneous increase in TOC. Mo/TOC on the other hand does not increase with the CIE from isotope stages T1 to T2. This section does not cover stages T3 to T5 where we observe an increase in Mo in the Yorkshire coast and RWK-01 sections. The sum of the geochemical parameters points to an intensification in the water column anoxia and transition to euxinia from the base of the Posidonia Formation (T1) to stage T2. A movement towards sulfidic water conditions has also been documented by the pyrite framboid size distribution in F11-01 and another Dutch Central Graben section L05-04 by Trabucho-Alexandre et al. (2012). However, the authors argued for commonly oxic conditions during the Toarcian CIE, based on observations of reworked sediment by strong currents and bioturbation. Although short incisions of oxic-dysoxic conditions on a seasonal to annual basis are conceivable and would not have been recorded by the sampling resolution in this study, the data at hand still indicates predominantly anoxic bottom water.

4.3. Organic-matter associations and palynological assemblages

AOM is a dominant constituent of the organofacies associations recorded during the CIE (Table S1). The understanding of the biological origin of microscopic AOM is problematic. Pacton et al. (2011) document, on the basis of studying an array of modern AOM-accumulations two different kinds of AOM. A light to dark-brown type with a granular aspect, which is a direct microbial product and can be found associated with filamentous bacterial filaments. The second type defined by Pacton et al. (2011) comprises dark-brown elements with a jellified aspect. Pacton et al. (2011) considered this to be related to terrestrial fragment degradation mediated by microorganisms. The latter type is consequently considered a secondary product of microbial activity. The AOM-particles recorded in this study bear more similarity to those with a granular aspect, albeit individual specimens differ in the density and consequently opacity. The specimens we observed are weakly fluorescent under UV-illumination, in a grey to slightly brownish colour spectrum. AOM with weak fluorescence has typically been considered as terrestrially-derived or strongly degraded phytoplankton organic-matter (see e.g., Tyson, 1987). The study by Pacton et al. (2011) shows that it could also be related to extracellular polymeric substances produced by microbes that bind different particles together. This would explain the entrapment of palynomorphs in the AOM clusters. Consequently, we hypothesize that relative enrichment of AOM is linked to increased microbial primary productivity. Higher proportions of wood-derived palynoclasts are indicative of a relative increase of terrestrial organic matter. This can either be linked to increased terrestrial runoff or a relative demise in AOM raindown.

Four groups of palynomorphs were identified. The first group constitutes organic-walled dinoflagellate cysts (dinocysts) that represent the resting cysts of a type of marine plankton that is observed in a wide array of marine environments. The fossil group appears in the Triassic and is known to have undergone rapid diversification from the Toarcian onward (Fensome et al., 1996). The second group consists of acritarchs, which are small algal cysts that cannot be attributed to either dinoflagellate cysts or resting cysts of known algae. In this study, the genera *Michrystridium* and *Veryachium* are abundantly present. The third group consists of prasinophyte algae, which are a class of primitive unicellular eukaryotic algae, with fossils dating back to the Cambrian (Anbar and Knoll, 2002; Knoll et al., 2006). They are represented by phycomata, which are episodically generated, relatively large organic-walled vegetative division cysts of various thickness. The taxonomy of these cysts has poorly evolved and centers around the smooth forms assignable to leiosphaerids and those with walls consisting of tubular channels, which are often assigned to *Pleurozonaria* and *Tasmanites* (Mädler, 1968). A high abundance of prasinophytes occurs when reactive nitrogen and phosphorus become freely available in the photic zone (Prauss, 2007; van de Schootbrugge et al., 2013). Stratification and photic-zone anoxia may contribute to nitrogen depletion in surface waters, favouring organisms with low requirements for nitrate (van de Schootbrugge et al., 2013). Such an ecological affinity has been shown in nitrogen-starved culture experiments with the prasinophyte *Micromonas pusilla*, which quickly reacts to increased levels of ammonium in the growth medium. This provides a mechanism for prasinophyte prosperity under photic zone anoxia (see Prauss, 2007; van de Schootbrugge et al., 2013). The fourth group consists of spheromorph algal cysts in which we have grouped relatively small spherical particles with no obvious ultrastructure such as spines, granules or openings. Larger specimens are typically referred to as *Leisosphaera*, whereas smaller (<10 μm) are known as *Halosphaeropsis liassica* (after Bucefalo Palliani et al., 2002). Their biological origin is unknown but they are usually thought to be juvenile phycomae, representing part of the life-cycle of prasinophyte algae (van de Schootbrugge et al., 2013). This assumption is supported by a UV-fluorescence behavior that is very similar to that of known prasinophytes like *Pleurozonaria*. The terrestrial palynomorphs were categorized into five main groups of predominant conifer pollen; *Chasmatosporites*, *Classopollis*, *Cerebropollenites* and other saccates pollen. Various trilete spores were also grouped. Other taxa were grouped in the "others" category.

4.3.1. Cleveland Basin - Yorkshire coast

In the upper part of the Grey Shale Member, corresponding to the initial phase of the CIE (isotope unit T1) organofacies associations comprise a mixture of palynomorphs (~50%), AOM Type-1 (40%) and wood remains (10%) (Fig. 6). The palynomorph assemblages in turn are relatively diverse, including polygonomorph and netromorph acritarchs (*Michrystridium* and *Leiofusa* spp., respectively), and sporomorphs (predominantly *Chasmatosporites* spp., bisaccate pollen and trilete spores). Small (~10 μm) UV-fluorescent spherical bodies, here referred to as *Halosphaeropsis liassica* are abundant in roughly equal proportions. Organic-walled dinoflagellates, predominantly *Nannoceratopsis* spp. are also present in abundance. Prasinophyte algae (predominantly *Tasmanites* and *Pleurozonaria* spp.) are recorded in low relative abundance. The combined assemblages are indicative of a combination, possibly on a seasonal scale, of oxygenated marine conditions as indicated by abundant organic-walled dinocysts and more adverse conditions likely affected by surface-water anoxia. The presence of *Halosphaeropsis liassica* suggests that enhanced stratification and possible surface-water anoxia existed periodically.

At the base of T2 AOM Type-1 becomes the dominant form (Fig. 6). Concomitantly, towards the base of the Jet Rock unit, acritarchs increase in abundance at the expense of *Halosphaeropsis liassica*. Sporomorphs (predominantly *Chasmatosporites* spp.) continue in stable abundance. Dinoflagellate cysts also persist up to the base of the Jet Rock unit. This indicates that comparable conditions as those during isotope stage T1 persisted.

For the lower 1.5 m of the Jet Rock unit (stage T2), organic-matter associations remain dominated by AOM. The palynomorph assemblages are characterized by a demise in the relative abundance of sporomorphs, with *Halosphaeropsis liassica* becoming the dominant palynomorph type. Remarkably, organic-walled dinoflagellate cysts are consistently abundant below the base of the Jet Rock. However, they undergo a decrease in abundance, coinciding with the first isotope shift just below the base of Jet Rock, to become completely absent at approximately 1 m above the base of the Jet Rock unit. This may be considered a consequence of stratification and surface-water deoxygenation. Although becoming less prominent in terms of total abundance, the sporomorph assemblages are characterized by a drastic increase of the *Classopollis* group in isotope stage T2.

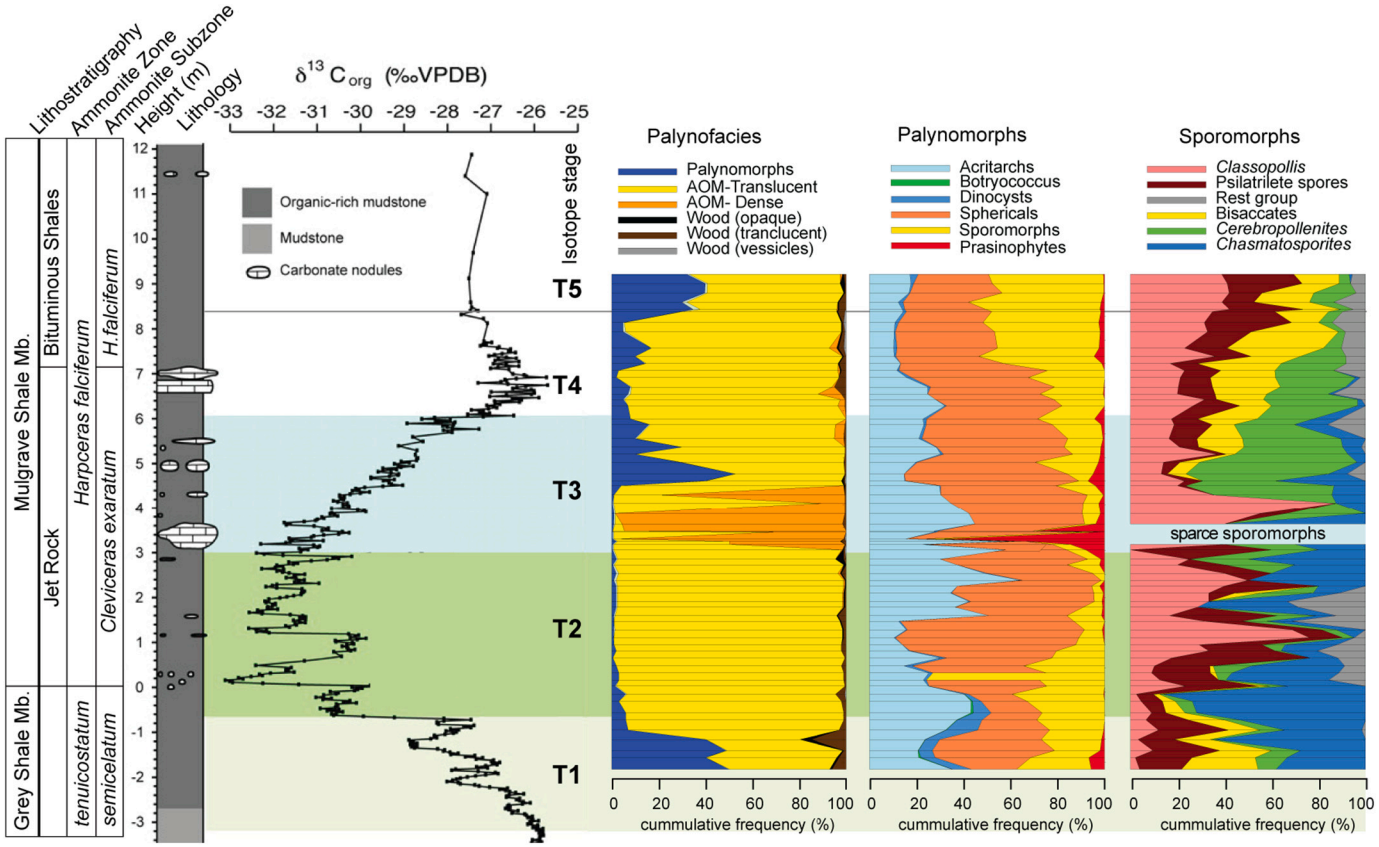

Fig. 6. Organic matter associations and palynological associations across the Lower Toarcian section from the Yorkshire Coast. The carbon isotope data is from Kemp et al. (2011). The isotope stages T1 to T5 provide stratigraphic context.

With the CIE-recovery (stage T3) we note a change in the organic-matter associations through the appearance of dense clusters of AOM, denoted as AOM Type-2, together with a transient dominance of large, thick-walled prasinophyte algae assigned to the genus *Pleurozonaria*. Remarkably, sporomorphs are virtually absent in this interval. We ascribe this to dilution by an apparently massive flux of prasinophyte algae, *Halosphaeropsis liassica* and acritarchs at this time.

In the middle of Stage T3, AOM Type-1 returns to be dominant in company of abundant palynomorphs (20–50%). This indicates that the postulated dilution by AOM rain-down diminished. Subsequently, the palynomorph assemblages remain dominated by *Halosphaeropsis liassica* and acritarchs. Sporomorphs progressively increase in abundance reaching ~20% at 6.5 m above the base of the Jet Rock. Interestingly, whereas in the lower half of the Jet Rock unit the sporomorph associations were dominated by *Chasmatosporites*, the upper half is dominated by *Cerebropollenites*. The organofacies associations remain dominated by AOM Type-1 during stage T4. Palynological assemblages are dominated by *Halosphaeropsis liassica* and acritarchs. Sporomorphs however, progressively increase in abundance constituting about 50% of the palynomorphs assemblage from interval T4 and into interval T5. Organic-walled dinoflagellate cysts are consistently present from now on. However, the assemblages no longer constitute the species *Luehndea spinosa*, which thus goes extinct across the T-OAE. The sporomorph associations are characterized by turnover from a *Cerebropollenites*-dominated assemblage to more prominent *Classopollis* and *Perinopollenites* spp..

4.3.2. West Netherlands Basin Well RWK-01

The base of the investigated core from Well RWK-01 lies just below a cemented fault that truncates the base of the CIE. Below the unconformity we record palynological assemblages that are dominated by sporomorphs, notably bisaccate conifer pollen and to a lesser extent *Chasmatosporites* spp. (Fig. 7). Given the presence of dinoflagellate cysts such as *Luehndea spinosa* and *Nannoceratopsis gracilis* a late Pliensbachian age is suggested for this interval. The lowermost sample from within the CIE corresponds to the CIE-plateau (isotope stage T2). Organofacies associations are now dominated by AOM. The palynomorph assemblage at this point is dominated by prasinophyte algae (*Pleurozonaria* spp.), thus likely corresponding to the same prasinophyte acme we recorded coevally in the Cleveland Basin. Subsequently, the organofacies associations also constitute the dense AOM Type-2 throughout isotope stage T2 and repeatedly through part of the CIE-recovery (isotope stage T3). Also, this return of AOM Type-2 is straddled by a prasinophyte acme. AOM Type-2 is recorded up to the top of the CIE-recovery. For the remainder of the interval spanning the CIE-recovery, *Halosphaeropsis liassica* remains overwhelmingly dominant. After the termination of the CIE and its characteristic 'overshoot' (isotope stage T4), acritarchs and organic-walled dinoflagellate cysts return at moderate abundance to become truly abundant substantially after the CIE at 2081 m depth. In essence, we record the same reorganisation among the terrestrial elements as in the Yorkshire Coast section, with a transition from *Chasmatosporites* to *Cerebropollenites* and back to *Chasmatosporites* after the CIE.

4.3.3. Dutch Central Graben Well F11-01

In Well F11-01 the onset and successive plateau phase of the CIE are recovered. At the base of the succession, across the initial isotope shift (isotope stage T1), we note a progressive shift towards the dominance of AOM at the expense of sporomorphs and wood-fragments (Fig. 8). In this interval organic-walled dinoflagellate cysts are still abundant alongside a relatively diverse assemblage of sporomorphs (predominantly *Chasmatosporites* spp.), prasinophyte algae, acritarchs and *Halosphaeropsis liassica*. Closer towards the isotope plateau phase, AOM Type-1 becomes

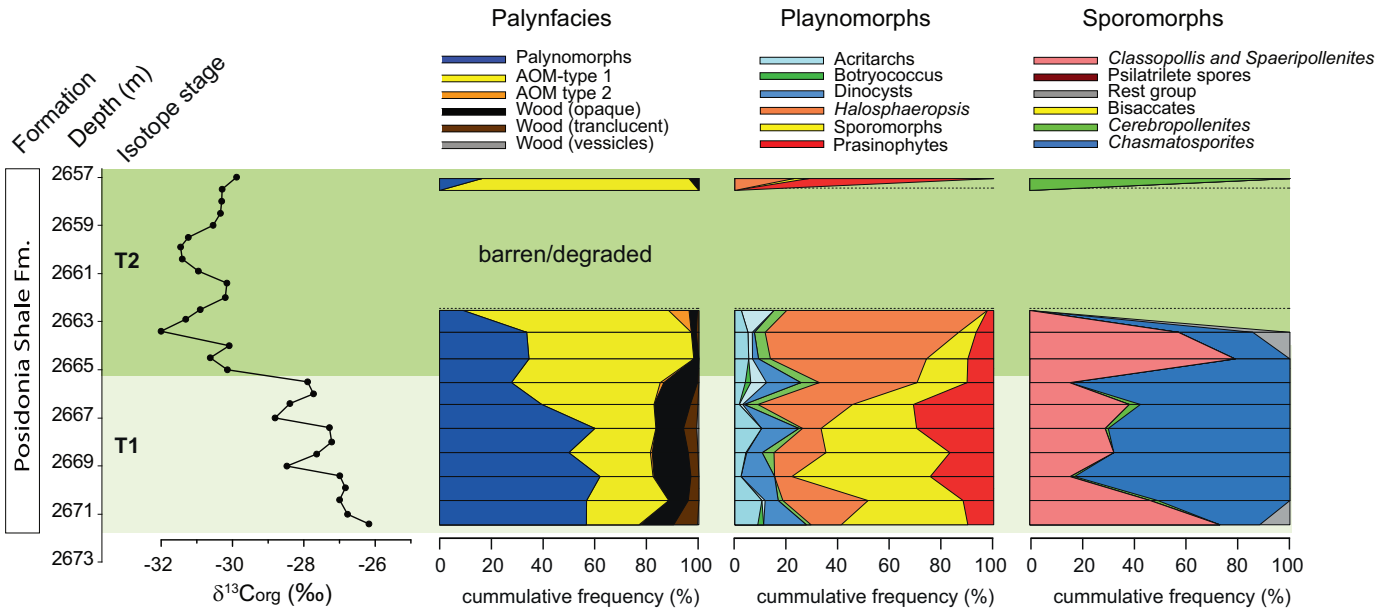

Fig. 7. Organic matter associations and palynological associations in the well F11-01, Dutch Central Graven. Only the onset of the CIE and its 'plateau phase' are recovered in this cored section. The isotope stages T1 and T2 provide stratigraphic context.

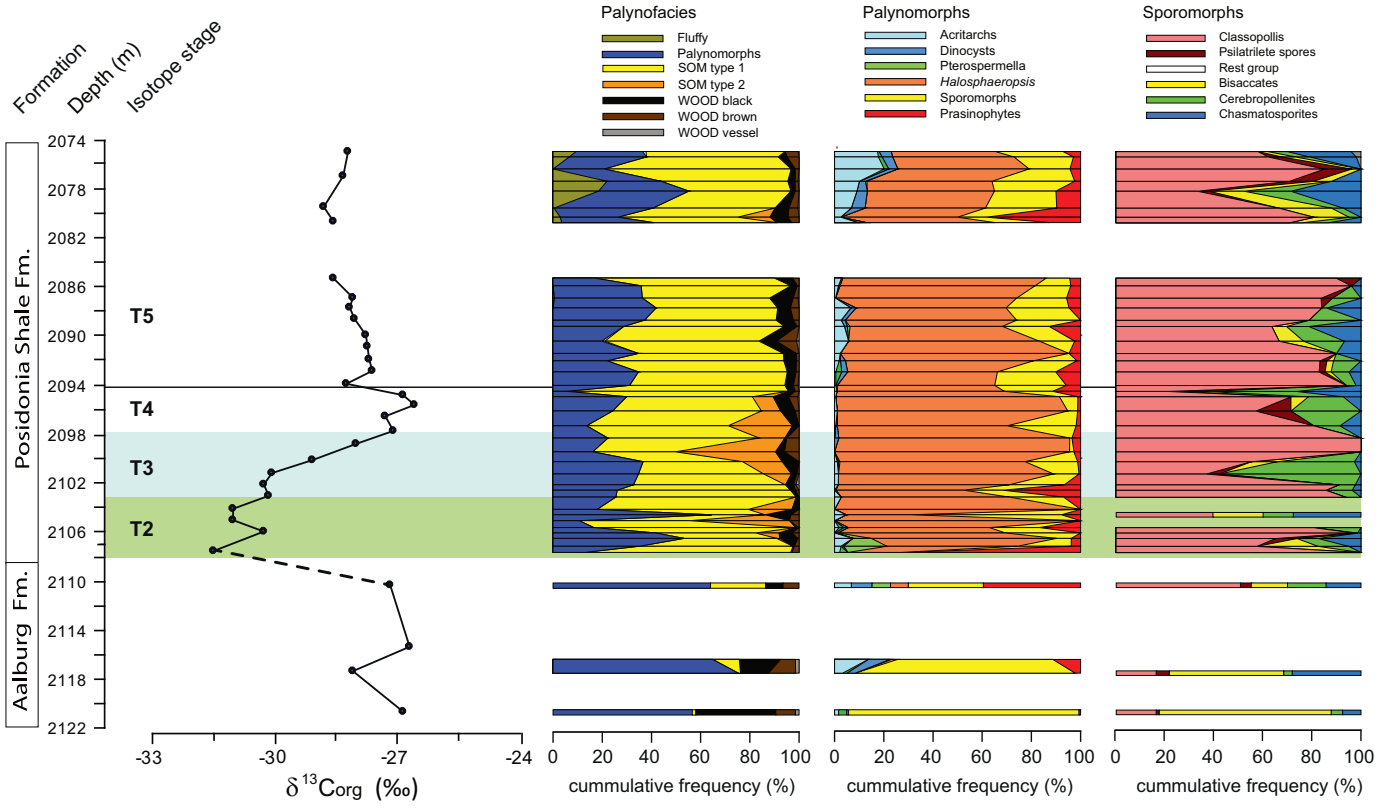

Fig. 8. Organic matter associations and palynological associations in well RWK-01. The base of the investigated interval is truncated by a fault. The isotope stages T2 to T5 provide stratigraphic context.

the dominant constituent of the organofacies and *Halosphaeropsis liassica* the dominant palynomorph. Organic-walled dinoflagellate cysts are now completely absent. The interval recovered from the 'isotope plateau' stage T2 are devoid of well-preserved organic matter. Only visual aggregates of bitumen-like material are recovered. This is also the interval in which the core is characterized by streaks of fibrous calcite or 'beef'. These structures are thought to be a late diagenetic phenomenon, principally caused by fluid overpressure (see Cobbold et al., 2013; Hooker et al., 2020). Hence, it appears that this specific interval is affected by hydrocarbon expulsion, which led to the destruction of the in-situ organic-matter associations. The uppermost sample from the core, in contrast, again yields palynological recovery. The organofacies

remains dominated by AOM. The palynomorph assemblage is dominated by prasinophyte algae that are also prominent in coeval sediments in the Yorkshire Coast and RWK-01 sections.

5. Discussion

The iron-speciation, that is dominated by reactive iron species, indicates that anoxic (ferruginous) bottom-water conditions were already established at the base of the CIE, prior to the rapid negative $\delta^{13}C$ shift, and persisted throughout and beyond the CIE at all studied localities (Figs. 3–5). A progressive shift to reducing conditions within the *semicelatum* to *exaratum* subzones, ranging from the base to the peak of the CIE was recorded in the geochemical records (e.g. McArthur et al., 2008; Remírez and Algeo, 2020a). We do not observe such a change in the Yorkshire Coast section where the Fe-speciation points to euxinic conditions being already at the base of the CIE. However, in the Dutch Central Graben (F11–01) a significant change from predominantly anoxic (ferruginous) euxinic bottom water conditions occurs from isotope stages T1 to T2. Indeed, pulses of anoxic/euxinic bottom water conditions were recorded before the onset of the CIE in the Grey Shale Member in the Yorkshire section (McArthur et al., 2008; Salem, 2013; Thibault et al., 2018; Remírez and Algeo, 2020a). Thallium isotopes as well as Fe-speciation results from sedimentary successions from the Western Canadian Sedimentary Basin and the eastern European shelf pointed to an establishment of bottom water anoxia starting from the Pliensbachian-Toarcian boundary and partly earlier (Them et al., 2018). Biomarkers provide evidence that not only the bottom water but also the photic zone had episodes of euxinia in the Yorkshire Coast section during the *semicelatum* Zone (French et al., 2014).

It appears that reducing bottom-water redox conditions existed prior to the CIE and did not commence with the rapid light carbon injection that occurred from isotope stage T1 to T2. The earlier onset of bottom water anoxia could have been related to an increase in continental runoff resulting in salinity stratification and/or progressive weakening of the ocean circulation and oxygen solubility driven by global warming and rising seawater temperature prior to the Toarcian CIE. However, evidence from osmium and oxygen isotopes clearly relates the enhanced weathering as well as high seawater temperatures directly to the Toarcian CIE (e.g., Cohen et al., 2007; Dera and Donnadieu, 2012; Kemp et al., 2020), negating the hypothesis. Nevertheless, a shift towards warmer seawater temperatures was noted at the Pleinsbachian/Toarcian boundary (Suan et al., 2008; Metodiev and Koleva-Rekalova, 2008; Slater et al., 2019). A development of brackish conditions in the Cleveland Basin was recorded by Remírez and Algeo, 2020a prior to the CIE. Them et al. (2017) also identify a positive spike in $^{187}Os/^{188}Os$ at the Pleinsbachian/Toarcian boundary, depicting an increased weathering pulse. It is possible that an initial increase in stratification and warming triggered bottom water anoxia that then persisted in the hydrographically restricted setting of the north-western EES with poor hydrological exchange (see McArthur et al., 2008; Ruvalcaba Baroni et al., 2018; Dickson et al., 2017).

The palynological and organofacies results, on the other hand, reveal pronounced changes in close relationship to the CIE and TOC. The base of the CIE marks a shift in the organofacies, with amorphous organic matter becoming dominant. In the light of recent in-vivo cultivation experiments (Pacton et al., 2011), the type of AOM that was recorded closely resembles that produced as extracellular polymeric substances by various bacteria. The relative abundance of the *Classopollis* sporomorph group that is considered to be a thermophilous gymnosperm pollen (van Konijnenburg-van Cittert and van der Burgh, 1996; Abbink et al., 2004) increases coevally with the CIE, which is a likely response to further climatic warming recorded during the T-OAE. Collectively, the palynological results suggest a major reorganisation of the marine ecosystem in conjunction with the T-OAE. Starting at the base of the CIE an increase in the relative abundance of prasinophycean vegetative cysts is recorded at all three sites, after which the spheromorph algal cysts attributed to *Halosphaeropsis liassica* remain dominant.

Both paleo- and actuobiological studies suggest that prasinophyte algae possess a strong preference for ammonium over nitrate (Cochlan and Harrison, 1991) and, consequently, can use ammonium released by nitrogen fixers as their own nitrogen source (Stumm and Morgan, 1981; Herrero et al., 2001). The correspondence between prasinophyte prosperity and AOM-dominated organofacies, which may be indicative of photo-autotrophic prokaryotes (e.g., cyanobacteria, green- and purple sulphur bacteria), could indicate a potential symbiosis between these groups. Chemocline and eventually euxinia shoaling into the photic zone could act as a key trigger for this symbiosis. Under this scenario, initial chemocline shoaling promoted the development and production of the larger prasinophyte vegetative cysts (*Tasmanites* and *Pleurozonia*). Subsequently, once the photic zone was largely euxinic, small short life-cycle vegetative cysts ascribed to *Halosphaeropsis liassica* were produced and exported.

We consequently hypothesize that the observed palynological and organofacies patterns are indicative of the establishment of an anoxygenic ecosystem with green-purple sulphur bacteria and/or cyanobacteria during the T-OAE, in response to photic zone anoxia and potentially photic zone euxinia. This is in-line with results based on specific organic molecular biomarkers for these anoxygenic photosynthesizing prokaryotes (Schouten et al., 2000; French et al., 2014). Particularly noteworthy is the apparently coeval intensification of the abovementioned anoxygenic productivity regime during the maximum $\delta^{13}C$ excursion stage (T3), where we note very dense AOM bracketed by the abundance of larger prasinophytes (Fig. 9). In the Cleveland Basin, this regime is terminated immediately after the recovery of the CIE (Fig. 6) since dilution of palynomorphs by AOM is no longer observed and dinoflagellate cysts return. In the West Netherlands Basin however, dinoflagellate cysts and more diverse organofacies associations return only after the CIE (Fig. 8). The organofacies trends in this study imply that oxygenation of the majority of the water column commenced in the Cleveland Basin, with the West Netherlands Basin following with a minor delay, whereas the geochemical record still points to mostly anoxic bottom water conditions at all locations but with sufficient water mass replenishment post CIE (i.e., increase in Mo/TOC; McArthur et al., 2008; Dickson et al., 2017; Remírez and Algeo, 2020a).

In terms of organic matter enrichment, the combined palynological and organic-matter characterization data indicate that primary productivity did not collapse during the T-OAE, and that organic-matter enrichment was not merely an effect of inhibited organic-matter remineralization under anoxic bottom-water conditions. In contrast, our observations support a scenario in which anoxygenic photosynthetic productivity proliferated in a stratified, nutrient-rich, anoxic and/or seasonally euxinic surface-water environment (see also Slater et al., 2019). At the same time, the geochemical redox indicators point to anoxic and intermittently euxinic conditions of the bottom-waters in all three sections. Although anoxic conditions contribute to preservation of organic matter, we observe that anoxia was not the dominant driver of elevated organic matter accumulation during T-OAE. The organofacies associations indicate vigorous primary productivity along with organic matter enrichments across northwestern Europe. Consequently, a larger supply of organic matter would have in return helped to sustain anoxic conditions (see also Slater et al., 2019). Concomitant with the redistribution of the organofacies, organic matter burial declined post T-OAE, exemplified by TOC values below 5%.

In summary, existing bottom water anoxia from the beginning of the CIE would have provided the ideal conditions for organic matter preservation, whereas the enhanced and likely predominantly anoxygenic primary productivity at peak CIE accelerated the amount of organic carbon production leading to increased organic matter burial.

6. Conclusions

The combination of high-resolution organofacies, palynological and

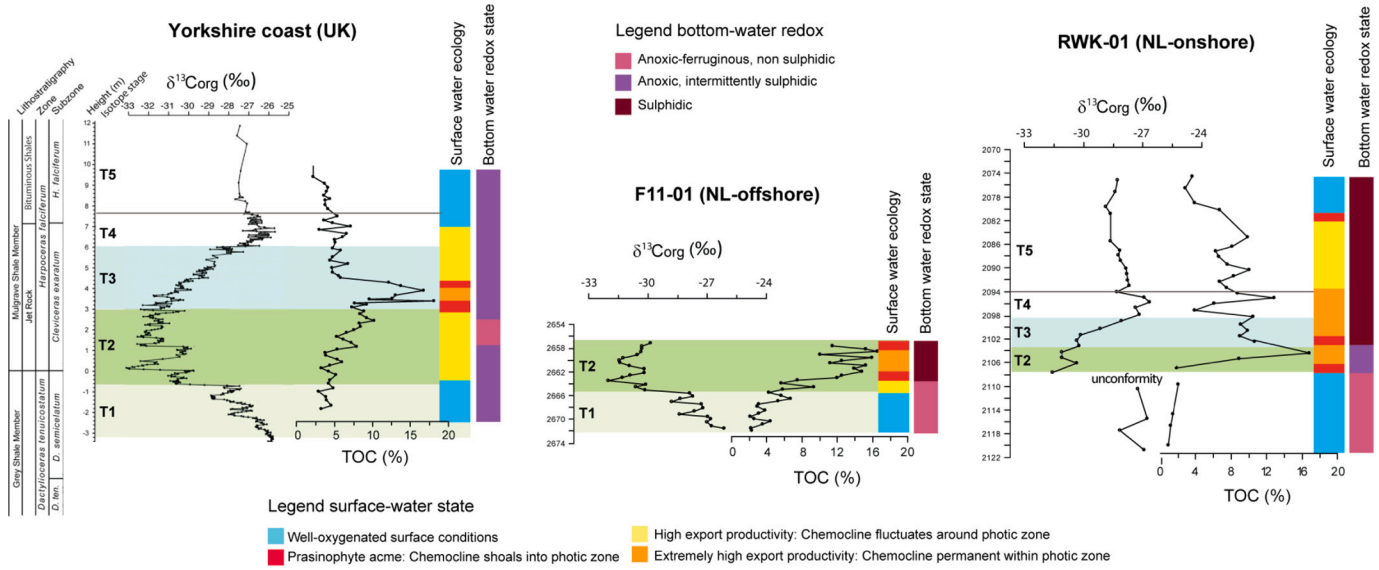

Fig. 9. Schematic representation of surface-water ecology (derived from palynological patterns) and bottom-water redox state (derived from iron speciation and redox-sensitive elements). T1 to T5 denote the isotope stages described in this study. The colour-bars on the right of each section represent the dominant and not the permanent mode.

geochemical data from three sections from the northwestern European Epicontinental Shelf enables a reconstruction of water column oxygenation and organofacies variations contributing to organic carbon burial during the T-OAE. Prior to the T-OAE (e.g., the *tenuicostatum* ammonite Zone), typical oxygenated shallow marine conditions persisted, with abundant organic-walled dinoflagellate cysts. Anoxic bottom water conditions, were already established on the NW European shelf. The interval from the base of the CIE to substantially beyond the recovery to pre-excursion $\delta^{13}C_{org}$ values is manifested by anoxic and intermittently euxinic bottom-water conditions whereas the surface waters are still largely oxygenated, as deduced from the organic and macrofossil assemblages and geochemical redox indicators.

A shift in organofacies at the base of the T-OAE (and its characteristic CIE) marks the onset of the dominance of amorphous organic matter as a consequence of increased marine and likely anoxygenic organic-matter production. This would have led to dilution of the background input of terrestrial organic-material. Mass occurrences of large prasinophyte algae pre- and postdate the interval with AOM dominance and the TOC-maxima, while Fe-speciation as well as other chemical redox indicators point to persistently anoxic to euxinic bottom water. Small vegetative cysts of prasinophyte algae (*Halosphaeropsis liassica*) are overwhelmingly dominant, suggesting that anoxic conditions reached into the photic zone at least periodically. At this stage, combined palynological and organic-matter data show that primary productivity did not collapse in response to photic zone anoxia. Instead, an ecosystem comprising anoxygenic photosynthesizers contributed to an elevated organic matter flux to the sediment, which was better preserved under the prevailing anoxic bottom-water conditions.

After the CIE, surface-waters became reoxygenated, as manifested by re-occurrence of dinocysts. Nevertheless, surface water anoxia likely occurred intermittently, as indicated by the persistent abundance of prasinophytes, *Halosphaeropsis* and AOM, whereas the bottom water remained largely anoxic. The trends in anoxia, primary productivity and organic matter deposition are recorded synchronously across large distances (>500 km) throughout the study area, with a minor delay in surface water oxygenation from the Cleveland Basin to the West Netherlands Basin.

Declaration of Competing Interest

The authors declare that they have no known competing financial interests or personal relationships that could have appeared to influence the work reported in this paper.

Acknowledgements

The data presented in this contribution were generated in an applied research project that was carried out by TNO and funded by Wintershall Noordzee B.V. and Energie Beheer Nederland (EBN) B.V. This project also received a subsidy from the Dutch Ministry of Economic Affairs, National Regulations EA-subsidies, Topsector Energy executed by the Netherlands Enterprise Agency. CS acknowledges funding from the Netherlands Organisation for Scientific Research (NWO Vici grant # 865.13.005). The authors thank Nico Janssen and Chris Martes for laboratory and analytical work, as well as Susanne Nelskamp and Roel Verreussel for helpful discussions. We also thank Stephen Hesselbo and two anonymous reviewers for their very constructive comments.

Appendix A. Supplementary data

Supplementary data to this article can be found online at https://doi.org/10.1016/j.palaeo.2020.110191.

References

Abbink, O., van Konijnenburg-van Cittert, J.H.A., Visscher, H., 2004. A sporomorph ecogroup model of the Northwest European Jurassic–Lower Cretaceous: concepts and framework. Geol. Mijnb. 83, 17–38.

Algeo, T.J., 2004. Can marine anoxic events draw down the trace-element inventory of seawater? Geology 32, 1057–1060.

Algeo, T.J., Ignall, E., 2007. Sedimentary C_{org}:P ratios, paleocean ventilation, and Phanerozoic atmospheric pO_2. Palaeogeogr. Palaeoclimatol. Palaeoecol. 256, 130–155.

Algeo, T.J., Liu, J., 2020. A re-assessment of elemental proxies for paleoredox analysis. Chem. Geol. 540, 119549.

Algeo, T.J., Lyons, T., 2006. Mo-total organic carbon covariation in modern anoxic marine environments: implications for analysis of paleoredox and paleohydrographic conditions. Paleoceanography 21. https://doi.org/10.1029/2004PA001112.

Anbar, A.D., Knoll, A.H., 2002. Proterozoic Ocean chemistry and evolution: a bioinorganic bridge? Science 297, 1137–1142.

Anderson, R.F., Fleisher, M.Q., Lehuray, A.P., 1989. Concentration, oxidation-state, and particulate flux of uranium in the Black-Sea. Geochim. Cosmochim. Acta 53, 2215–2224.
Anderson, T.F., Raiswell, R., 2004. Sources and mechanisms for the enrichment of highly reactive iron in euxinic Black Sea sediments. Am. J. Sci. 304, 203–233.
Barclay, R.S., McElwain, J.C., Sageman, B.B., 2010. Carbon sequestration activated by a volcanic CO2 pulse during Ocean Anoxic Event 2. Nat. Geosci. 3, 205–208.
Bjerrum, C.J., Surlyk, F., Callomon, J.H., Slingerland, R.L., 2001. Numerical paleoceanographic study of the Early Jurassic transcontinental Laurasian Seaway. Paleoceanography 16 (4), 390–404.
Bowden, S.A., Farrimond, P., Snape, C.E., Love, G.D., 2006. Compositional differences in biomarker constituents of the hydrocarbon, resin, asphaltene and kerogen fractions: an example from the Jet Rock (Yorkshire, UK). Org. Geochem. 37 (3), 369–383.
van Breugel, Y., Baas, M., Schouten, S., Mattioli, E., Sinninghe Damsté, J.S., 2006. Isorenieratane record in black shales from the Paris Basin, France: Constraints on recycling of respired CO2 as a mechanism for negative carbon isotope shifts during the Toarcian oceanic anoxic event. Paleoceanography 21 (4).
Brumsack, H.-J., Gieskes, J.M., 1983. Interstitial water trace metal chemistry of laminated sediments from the Gulf of California, Mexico. Mar. Chem. 14, 89–106.
Bucefalo Palliani, R., Mattioli, E., Riding, J.B., 2002. The response of marine phytoplankton and sedimentary organic matter to the early Toarcian (Lower Jurassic) oceanic anoxic event in northern England. Mar. Micropaleontol. 46 (3), 223–245.
Canfield, D.E., Raiswell, R., Westrich, J.T., Reaves, C.M., Berner, R.A., 1986. The use of chromium reduction in the analysis of reduced inorganic sulfur in sediments and shales. Chem. Geol. 54, 149–155.
Chappaz, A., Lyons, T.W., Gregory, D.D., Reinhard, C.T., Gill, B., Li, C., Large, R.R., 2014. Does pyrite act as an important host for molybdenum in modern and ancient euxinic sediments? Geochim. Cosmochim. Acta 126, 112–122.
Clarkson, M., Poulton, S., Wood, R., Guilbaud, R., 2014. Assessing the utility of Fe/Al and Fe-speciation to record water column redox conditions in carbonate-rich sediments. Chem. Geol. 382, 111–122.
Cobbold, P.R., Zanella, A., Rodrigues, N., Løseth, H., 2013. Bedding-parallel fibrous veins (beef and cone-in-cone): worldwide occurrence and possible significance in terms of fluid overpressure, hydrocarbon generation and mineralization. Mar. Pet. Geol. 43, 1–20.
Cochlan, W.P., Harrison, P.J., 1991. Inhibition of nitrate uptake by ammonium and urea in the eucaryotic picoflagellate *Micromonas pusilla* (Butcher) Manton et Parke. J. Exp. Mar. Biol. Ecol. 153 (2), 143–152.
Cohen, A.S., Coe, A.L., Harding, S.M., Schwark, L., 2004. Osmium isotope evidence for the regulation of atmospheric CO2 by continental weathering. Geology 32 (2), 157–160.
Cohen, A.S., Coe, A.L., Kemp, D.B., 2007. The Late Palaeocene–Early Eocene and Toarcian (Early Jurassic) carbon isotope excursions: a comparison of their time scales, associated environmental changes, causes and consequences. J. Geol. Soc. 164 (6), 1093–1108.
Coleman, M.L., Raiswell, R., 1981. Carbon, oxygen and sulphur isotope variations in concretions from the Upper Lias of NE England. Geochim. Cosmochim. Acta 45 (3), 329–340.
Correia, V.F., Riding, J.B., Duarte, L.V., Fernandes, P., Pereira, Z., 2017. The palynological response to the Toarcian Oceanic Anoxic Event (Early Jurassic) at Peniche, Lusitanian Basin, western Portugal. Mar. Micropaleontol. 137, 46–63.
Danise, S., Twitchett, R.J., Little, C.T.S., Clémence, M.E., 2013. The impact of global warming and anoxia on marine benthic community dynamics: an example from the Toarcian (Early Jurassic). PLoS One 8, e56255.
Demaison, G.J., Moore, G.T., 1980. Anoxic environments and oil source bed genesis. AAPG Bull. 64, 1179–1209.
Dera, G., Donnadieu, Y., 2012. Modeling evidences for global warming, Arctic seawater freshening, and sluggish oceanic circulation during the Early Toarcian anoxic event. Paleoceanography 27.
Dickson, A.J., Gill, B.C., Ruhl, M., Jenkyns, H.C., Porcelli, D., Idiz, E., 2017. Molybdenum-isotope chemostratigraphy and paleoceanography of the Toarcian Oceanic Anoxic Event (Early Jurassic). Paleoceanog. Paleoclimate 32, 813–829.
Doornenbal, J.C., Stevenson, A.G. (Eds.), 2010. Petroleum Geological Atlas of the Southern Permian Basin Area. EAGE Publications B.V., Houten (342 pp.).
Fantasia, A., Föllmi, K.B., Adatte, T., Bernárdez, E., Spangenberg, J.E., Mattioli, E., 2018. The Toarcian oceanic anoxic event in southwestern Gondwana: an example from the Andean basin, northern Chile. J. Geol. Soc. 175 (6), 883–902.
Fensome, R.A., MacRae, R., Moldowan, J.M., Taylor, F.J.R., Williams, G.L., 1996. The early Mesozoic radiation of dinoflagellates. Paleobiology 22, 329–338.
French, K.L., Sepulveda, J., Trabucho-Alexandre, J., Gröcke, D.R., Summons, R.E., 2014. Organic geochemistry of the early Toarcian oceanic anoxic event in Hawsker Bottoms, Yorkshire, England. Earth Planet. Sci. Lett. 390, 116–127.
Ghadeer, S.G., Macquaker, J.H.S., 2011. Sediment transport processes in an ancient mud-dominated succession: a comparison of processes operating in marine offshore settings and anoxic basinal environments. J. Geol. Soc. Lond. 168, 835–846.
Goldberg, T., Poulton, S.W., Wagner, T., Kolonic, S., Rehkämper, M., 2016. Mo drawdown during Cretaceous Anoxic Event 2. Earth Planet. Sci. Lett. 440, 81–91.
Gómez, J.J., Goy, A., 2011. Warming-driven mass extinction in the Early Toarcian (Early Jurassic) of northern and central Spain. Correlation with other time-equivalent European sections. Palaeogeogr. Palaeoclimatol. Palaeoecol. 306, 176–195.
Hallam, A., 1962. A band of extraordinary calcareous concretions in the Upper Lias of Yorkshire, England. J. Sediment. Res. 32 (4), 840–847.
Helz, G.R., Vorlicek, T.P., Kahn, M.D., 2004. Molybdenum scavenging by iron monosulfide. Environ. Sci. Technol. 38, 4263–4268.
Hermoso, M., Minoletti, F., Pellenard, P., 2013. Black shale deposition during Toarcian super-greenhouse driven by sea level. Clim. Past 9, 2703–2712.
Herrero, A., Muro-Pastor, A.M., Flores, E., 2001. Nitrogen control in cyanobacteria. J. Bacteriol. 183 (2), 411–425.
Hesselbo, S.P., Jenkyns, H.C., 1995. A comparison of the Hettangian to Bajocian successions of Dorset and Yorkshire. In: Taylor, P.D. (Ed.), Field Geology of the British Jurassic. Geological Society, London, pp. 105–150.
Hesselbo, S.P., Gröcke, D.R., Jenkyns, H.C., Bjerrum, C.J., Farrimond, P., Bell, H.S.M., Green, O.R., 2000. Massive dissociation of gas hydrate during a Jurassic oceanic anoxic event. Nature 406, 392–395.
Hooker, J.N., Ruhl, M., Dickson, A.J., Hansen, L.N., Idiz, E., Hesselbo, S.P., Cartwright, J., 2020. Shale anisotropy and natural hydraulic fracture propagation: an example from the Jurassic (Toarcian) Posidonienschiefer, Germany. J. Geophys. Res. Solid Earth 125 (3), e2019JB018442.
Ingall, E.D., Bustin, R.M., van Cappellen, P., 1993. Influence of water column anoxia on the burial and preservation of carbon and phosphorus in marine shales. Geochim. Cosmochim. Acta 57, 303–316.
Izumi, K., Kemp, D.B., Itamiya, S., Inui, M., 2018. Sedimentary evidence for enhanced hydrological cycling in response to rapid carbon release during the early Toarcian oceanic anoxic event. Earth Planet. Sci. Lett. 481, 162–170.
Jenkyns, H.C., 1988. The early Toarcian (Jurassic) anoxic event; stratigraphic, sedimentary and geochemical evidence. Am. J. Sci. 288 (2), 101–151.
Jenkyns, H.C., 2010. Geochemistry of oceanic anoxic events. Geochem. Geophys. Geosyst. 11.
Jenkyns, H.C., Gröcke, D.R., Hesselbo, S.P., 2001. Nitrogen isotope evidence for water mass denitrification during the early Toarcian oceanic anoxic event. Paleoceanography 16, 593–603.
Keeling, R.F., Kortzinger, A., Gruber, N., 2010. Ocean deoxygenation in a warming world. Annu. Rev. Mar. Sci. 2, 199–229.
Kemp, D.B., Coe, A.L., Cohen, A.S., Schwark, L., 2005. Astronomical pacing of methane release in the Early Jurassic period. Nature 437 (7057), 396–399.
Kemp, D.B., Coe, A.L., Cohen, A.S., Weedon, G.P., 2011. Astronomical forcing and chronology of the early Toarcian (Early Jurassic) oceanic anoxic event in Yorkshire, UK. Paleoceanography 26 (4).
Kemp, D.B., Selby, D., Izumi, K., 2020. Direct coupling between carbon release and weathering during the Toarcian oceanic anoxic event. Geology 48, 976–980.
Knoll, A.H., Javaux, E.J., Hewitt, D., Cohen, P., 2006. Eukaryotic organisms in Proterozoic oceans. Philosophical Trans. Royal Soc B: Biol. Sci. 361 (1470), 1023–1038.
van Konijnenburg-van Cittert, J.H.A., van der Burgh, J., 1996. Review of the Kimmeridgian flora of Sutherland, Scotland, with reference to the ecology and in situ pollen and spores. Proc. Geol. Assoc. 107 (2), 97–105.
Korte, C., Hesselbo, S.P., Ullmann, C.V., Dietl, G., Ruhl, M., Schweigert, G., Thibault, N., 2015. Jurassic climate mode governed by ocean gateway. Nat. Commun. 6 (10), 015.
Kraal, P., Slomp, C.P., de Lange, G.J., 2010. Sedimentary organic carbon to phosphorus ratios as a redox proxy in Quaternary records from the Mediterranean. Chem. Geol. 277, 167–177.
Kuypers, M.M.M., Pancost, R.D., Nijenhuis, I.A., Sinninghe Damsté, J.S., 2002. Enhanced productivity led to increased organic carbon burial in the euxinic North Atlantic basin during the late Cenomanian oceanic anoxic event. Paleoceanography 17 (4), 1051. https://doi.org/10.1029/2000PA000569.
Mädler, K., 1968. Die figurierten organischen Bestandteile der Posidonienschiefer. Beihefte zum Geologischen Jahrbuch 58, 287–406.
März, C., Poulton, S.W., Beckmann, B., Küster, K., Wagner, T., Kasten, S., 2008. Redox sensitivity of P cycling during marine black shale formation: Dynamics of sulfidic and anoxic, non-sulfidic bottom waters. Geochim. Cosmochim. Acta 72, 3703–3717.
McArthur, J.M., Algeo, T.J., van de Schootbrugge, B., Li, Q., Howarth, R.J., 2008. Basinal restriction, black shales, Re–Os dating, and the Early Toarcian (Jurassic) oceanic anoxic event. Paleoceanography 23, PA4217. https://doi.org/10.1029/2008PA001607.
McElwain, J.C., Wade-Murphy, J., Hesselbo, S.P., 2005. Changes in carbon dioxide during an oceanic anoxic event linked to intrusion into Gondwana coals. Nature 435 (7041), 479–482.
Metodiev, L., Koleva-Rekalova, E., 2008. Stable isotope records ($\delta^{18}O$ and $\delta^{13}C$) of Lower-Middle Jurassic belemnites from the Western Balkan mountains (Bulgaria): palaeoenvironmental application. Appl. Geochem. 23, 2845–2856.
Montero-Serrano, J.-C., Föllmi, K.B., Adatte, T., Spangenberg, J.E., Tribovillard, N., Fantasia, A., Suan, G., 2015. Continental weathering and redox conditions during the early Toarcian Oceanic Anoxic Event in the northwestern Tethys: insight from the Posidonia Shale section in the Swiss Jura Mountains. Palaeogeogr. Palaeoclimatol. Palaeoecol. 429, 83–99.
Mort, H.P., Adatte, T., Keller, G., Bartels, D., Föllmi, K.B., Steinmann, P., Berner, Z., Chellai, E.H., 2008. Organic carbon deposition and phosphorus accumulation during Oceanic Anoxic Event 2 in Tarfaya. Morocco. Cretac. Res. 29, 1008–1023.
Pacton, M., Gorin, G.E., Vasconcelos, C., 2011. Amorphous organic matter—Experimental data on formation and the role of microbes. Rev. Palaeobot. Palynol. 166 (3–4), 253–267.
Pearce, C.R., Cohen, A., Coe, A.L., Burton, K.W., 2008. Molybdenum isotope evidence for global ocean anoxia coupled with perturbations to the carbon cycle during the Early Jurassic. Geology 36, 231–234.
Pedersen, T.F., Calvert, S.E., 1990. Anoxia vs. productivity: what controls the formation of organic-carbon-rich sediments and sedimentary rocks? AAPG Bull. 74, 454–472.
Percival, L.M.E., Cohen, A.S., Davies, M.K., Dickson, A.J., Hesselbo, S.P., Jenkyns, H.C., Leng, M.J., Mather, T.A., Storm, M.S., Xu, W., 2016. Osmium isotope evidence for two pulses of increased continental weathering linked to Early Jurassic volcanism and climate change. Geology 44 (9), 759–762. https://doi.org/10.1130/G37997.1.

Poulton, S.W., Canfield, D.E., 2005. Development of a sequential extraction procedure for iron: implications for iron partitioning in continentally derived particulates. Chem. Geol. 214, 209–221.
Poulton, S.W., Canfield, D.E., 2011. Ferruginous conditions: a dominant feature of the ocean through Earth's history. Elements 7, 107–112.
Poulton, S.W., Raiswell, R., 2002. The low-temperature geochemical cycle of iron: from continental fluxes to marine sediment deposition. Am. J. Sci. 302, 774–805.
Powell, J.H., 2010. Jurassic sedimentation in the Cleveland Basin: a review. Proc. Yorks. Geol. Soc. 58, 21–72.
Prauss, M., Riegel, W., 1989. Evidence from phytoplankton associations for causes of black shale formation in epicontinental seas. In: Neues Jahrbuch für Geologie und Paläontologie-Monatshefte, pp. 671–682.
Prauss, M.L., 2007. Availability of reduced nitrogen chemospecies in the photic zone waters as the ultimate cause for fossil prasinophyte prosperity. Palaios 22, 489–499.
Raiswell, R., Canfield, D.E., 1998. Sources of iron for pyrite formation in marine sediments. Am. J. Sci. 298, 219–245.
Remírez, M.N., Algeo, T.J., 2020a. Paleosalinity determination in ancient epicontinental seas: a case study of the T-OAE in the Cleveland Basin (UK). Earth Sci. Rev. 201, 103072.
Remírez, M.N., Algeo, T.J., 2020b. Carbon-cycle changes during the Toarcian (Early Jurassic) and implications for regional versus global drivers of the Toarcian oceanic anoxic event. Earth Sci. Rev. 209, 103283.
Röhl, H.J., Schmid-Röhl, A., Oschmann, W., Frimmel, A., Schwark, L., 2001. The Posidonia Shale (Lower Toarcian) of SW-Germany: an oxygen-depleted ecosystem controlled by sea level and palaeoclimate. Palaeogeogr. Palaeoclimatol. Palaeocol. 165, 27–52.
Ruebsam, W., Muller, T., Kovacs, J., Palfy, J., Schwark, L., 2018. Environmental response to the early Toarcian carbon cycle and climate perturbations in the northeastern part of the West Tethys shelf. Gondwana Res. 59, 144–158.
Ruebsam, W., Mayer, B., Schwark, L., 2019. Cryosphere carbon dynamics control early Toarcian global warming and sea level evolution. Glob. Planet. Chang. 172, 440–453.
Ruvalcaba Baroni, I., Pohl, A., van Helmond, N.A.G.M., Papadomanolaki, N.M., Coe, A. L., Cohen, A.S., van de Schootbrugge, B., Donnadieu, Y., Slomp, C.P., 2018. Ocean Circulation in the Toarcian (Early Jurassic): a Key Control on Deoxygenation and Carbon Burial on the European Shelf. Paleoceanog. Paleoclimatol. 33, 994–1012.
Salem, N.-E., 2013. Geochemical characterisation of the Pliensbachian-Toarcian boundary during the onset of the Toarcian Oceanic Anoxic Event. Thesis, School of Civil Engineering and Geosciences, Newcastle University, UK, North Yorkshire, UK (276 pp.).
van de Schootbrugge, B., Bachan, A., Suan, G., Richoz, S., Payne, J.L., 2013. Microbes, mud and methane: cause and consequence of recurrent early Jurassic anoxia following the end-triassic mass extinction. Palaeontology 56, 685–709.
van de Schootbrugge, B., Houben, A.J.P., Ercan, F., Verreussel, R., Kerstholt, S., Janssen, N.M.M., Nikitenko, B., Suan, G., 2019. Enhanced Arctic-Tethys connectivity ending the Toarcian Oceanic Anoxic Event in NW Europe. Geol. Mag. 157, 1593–1611.
Schouten, S., van Kaam-Peters, H.M., Rijpstra, W.I.C., Schoell, M., Damste, J.S.S., 2000. Effects of an Oceanic Anoxic Event on the stable carbon isotopic composition of early Toarcian carbon. Am. J. Sci. 300 (1), 1–22.
Slater, S.M., Twitchett, R.J., Danise, S., Vajda, V., 2019. Substantial vegetation response to Early Jurassic global warming with impacts on oceanic anoxia. Nat. Geosci. https://doi.org/10.1038/s41561-019-0349-z.
Stramma, L., Johnson, G.C., Sprintall, J., Mohrholz, V., 2008. Expanding oxygen–minimum zones in the tropical oceans. Science 320, 655–658. https://doi.org/10.1126/science.1153847.
Stumm, W., Morgan, J.J., 1981. Aquatic Chemistry: An Introduction Emphasizing Chemical Equilibria in Natural Waters, 2nd edn. John Wiley Sons Ltd., New York.
Suan, G., Mattioli, E., Pittet, B., Mailliot, S., Lecuyer, C., 2008. Evidence for major environmental perturbation prior to and during the Toarcian (Early Jurassic) oceanic anoxic event from the Lusitanian Basin, Portugal. Paleoceanography 23, PA1202. https://doi.org/10.1029/2007PA001459.
Suan, G., Nikitenko, B.L., Rogov, M.A., Baudin, F., Spangenberg, J.E., Knyazev, V.G., Glinskikh, L.A., Goryacheva, A.A., Adatte, T., Riding, J.B., Föllmi, K.B., Pittet, B., Mattioli, E., Lecuyer, C., 2011. Polar record of Early Jurassic massive carbon injection. Earth Planet. Sci. Lett. 312 (1–2), 102–113.
Summons, R.E., Powell, T.G., 1987. Identification of aryl isoprenoids in source rocks and crude oils: biological markers for the green sulphur bacteria. Geochim. Cosmochim. Acta 51 (3), 557–566.
Taylor, S.R., McLennan, S.M., 1985. The Continental Crust: Its Composition and Evolution. Blackwell, Oxford (312 pp.).
Tessin, A., Sheldon, N.D., Hendy, I., Chappaz, A., 2016. Iron limitation in the Western Interior Seaway during the Late Cretaceous OAE 3 and its role in phosphorus recycling and enhanced organic matter preservation. Earth Planet. Sci. Lett. 449, 135–144.
Them, T.R., Gill, B.C., Caruthers, A.H., Gröcke, D.R., Tulsky, E.T., Martindale, R.C., Poulton, T.P., Smith, P.L., 2017a. High-resolution carbon isotope records of the Toarcian Oceanic Anoxic Event (Early Jurassic) from North America and implications for the global drivers of the Toarcian carbon cycle. Earth Planet. Sci. Lett. 459, 118–126.
Them, T.R., Gill, B.C., Selby, D., Gröcke, D.R., Friedman, R., Owens, J.D., 2017b. Evidence for rapid weathering response to climatic warming during the Toarcian Oceanic Anoxic Event. Sci. Rep. 7, 5003.
Them, T.R., Gill, B.C., Caruthers, A.H., Gerhardt, A.M., Gröcke, D.R., Marroqín, S.M., Lyons, T.W., Nielsen, S.G., Trabucho Alexandre, J.P., Owens, J.D., 2018. Thallium isotopes reveal protracted anoxia during the Toarcian (Early Jurassic) associated with volcanism, carbon burial, and mass extinction. Proc. Natl. Acad. Sci. 115, 6596–6601.
Thibault, N., Ruhl, M., Ullmann, C.V., Korte, C., Kemp, D.B., Grocke, D.R., Hesselbo, S.P., 2018. The wider context of the lower Jurassic Toarcian oceanic anoxic event in Yorkshire coastal outcrops, UK. Proc. Geol. Assoc. 129 (3), 372–391.
TNO-GDN, 2020. Altena group. In: Stratigrafische Nomenclator van Nederland, TNO – Geologische Dienst Nederland. Consulted on 17–11–2020 on. http://www.dinoloket.nl/stratigrafische-nomenclator/altena-groep.
Trabucho-Alexandre, J., Dirkx, R., Veld, H., Klaver, G., de Boer, P.L., 2012. Toarcian black shales in the Dutch Central Graben: record of energetic, variable depositional conditions during an oceanic anoxic event. J. Sediment. Res. 82 (2), 104–120.
Tribovillard, N., Algeo, T.J., Lyons, T.W., Riboulleau, A., 2006. Trace metals as paleoredox and paleoproductivity proxies: an update. Chem. Geol. 232, 12–32.
Tsandev, I., Slomp, C.P., 2009. Modeling phosphorus cycling and carbon burial during Cretaceous Oceanic Anoxic Events. Earth Planet. Sci. Lett. 286, 71–79.
Tyson, R.V., 1987. The genesis and palynofacies characteristics of marine petroleum source rocks. In: Marine Petroleum Source Rocks, vol. 26. Blackwell Scientific Publications, Oxford, pp. 47–67.
Wignall, P.B., 1994. Black Shales. In: Oxford Monographs on Geology and Geophysics, no. 30. Oxford University Press.
Wignall, P.B., Hallam, A., 1991. Biofacies, stratigraphic distribution and depositional models of British onshore Jurassic black shales. Geol. Soc. Lond., Spec. Publ. 58, 291–309.
Xu, W., Ruhl, M., Jenkyns, H.C., Hesselbo, S.P., Riding, J.B., Selby, D., Naafs, B.D.A., Weijers, J.W.H., Pancost, R.D., Tegelaar, E.W., Idiz, E.F., 2017. Carbon sequestration in an expanded lake system during the Toarcian oceanic anoxic event. Nat. Geosci. 10, 1–7.
Zheng, Y., Anderson, R.F., van Geen, A., Kuwabara, J., 2000. Authigenic molybdenum formation in marine sediments: a link to pore water sulphide in the Santa Barbara Basin. Geochim. Cosmochim. Acta 64, 4165–4178.